Retraction for *Analyst*:

Retracted article: Ionic liquid-functionalized graphene for fabricating an amperometric acetylcholinesterase biosensor

Yanping Li and Gaoyi Han

Analyst, 2012 (DOI: 10.1039/ C2AN35065C). **Retraction published 21st August 2013**

The authors hereby wholly retract this *Analyst* paper due to the significant overlap in the text with an article published in *Analytica Chimica Acta* at an earlier date. The authors acknowledge that whilst the data in the article are unique and true, the overlap in the text is extensive and they are retracting this article to maintain the accuracy of the scientific record.

This retraction is endorsed by May Copsey, Editor. Retraction published 21st August 2013.

Analyst

Dynamic Article Links

Cite this: *Analyst*, 2012, **137**, 3160

www.rsc.org/analyst

PAPER

Ionic liquid-functionalized graphene for fabricating an amperometric acetylcholinesterase biosensor†

Yanping Li and Gaoyi Han*

Received 13th January 2012, Accepted 18th April 2012
DOI: 10.1039/c2an35065c

This work reports a sensitive amperometric biosensor for organophosphate pesticides (OPs) fabricated by modifying a glassy carbon electrode with acetylcholinesterase (AChE) immobilized on ionic liquid-functionalized graphene (IL-G). The functionalized graphene sheets had good dispersibility and long-term stability in various solvents. The as-prepared biosensor showed high affinity to acetylthiocholine (ATCl) with a Michaelis–Menten constant (K_m) value of 0.77 mM. Furthermore, based on the inhibition by OPs of the enzymatic activity of the immobilized AChE, and using carbaryl as a model compound, the inhibition of carbaryl was proportional to its concentration ranging from 0.0025 to 0.48 and 0.48 to 1.42 μg mL^{-1} with a detection limit of 0.8 ng mL^{-1} ($S/N = 3$). The developed biosensor exhibited a good performance for OPs detection, including good reproducibility and acceptable stability, which provided a new and promising tool for the analysis of enzyme inhibitors.

Introduction

In recent years, the extensive utilization of organophosphorus pesticides (OPs) for pest control has raised serious public concern regarding health, the environment and food safety.[1,2] Therefore, rapid determination and reliable quantification of trace levels of OPs compounds have become increasingly important for public security and health protection. Many techniques such as gas or liquid chromatography and mass spectroscopy have been introduced for monitoring trace levels of these compounds.[3] Although these instrumental methods for pesticide determination are accurate, they require complicated pretreatment steps, extensive labor resources, and are not applicable for on-site determination. Meanwhile, enzyme-based biosensors, which represent good selectivity, sensitivity, rapid response, and miniature size, have emerged as a promising alternative to detect pesticides.[4] Among them, electrochemical acetylcholinesterase (AChE) biosensors based on the inhibition of AChE have shown satisfactory results for pesticide analysis when the enzyme activity is employed as an indicator for quantitative measurement of insecticides.[5,6] When AChE is immobilized on the working electrode surface, its interactions with the substrate acetylthiocholine chloride (ATCl) produce the electro-active product of thiocholine, and the inhibition of the enzyme system can be monitored by measuring the oxidation current of thiocholine.[7] As an alternative strategy, many nanomaterials including gold nanoparticles (AuNPs), carbon nanotubes and so on have been employed to fabricate AChE biosensors with good performance including high sensitivity, rapid response and good stability.[8–12]

Graphene, considered as a "rising star" nanostructured carbon material, is a flat monolayer of carbon atoms tightly packed into a two-dimensional honeycomb lattice, and a basic building block for graphitic materials of all other dimensionalities such as carbon nanotubes and fullerenes.[13] Because of their novel properties,[14,15] such as exceptionally high electrical conductivity, and thermal and mechanical properties, graphene sheets have received considerable interest for potential applications in the fields of nanocomposites,[16,17] nanoelectronics[18] and electromechanical resonators.[19] The biological applications of graphene, such as a DNA-hybridization device and in delivery of drugs, have also started to attract interest.[20–24] For example, Dai *et al.* have synthesized nanoscale graphene oxide sheets by branched polyethylene glycol (PEG) and found a unique ability of graphene in the attachment and delivery of aromatic, water-insoluble drugs.[21] Mohanty and Berry fabricated a novel graphene-based live-bacterial-hybrid device and a DNA hybridization device with excellent sensitivity.[22] A CdS-decorated graphene nanocomposite,[25] a TiO_2-decorated graphene nanohybrid,[26] a nanohybrid containing gold nanoparticles and chemically reduced graphene oxide nanosheets[27] and 3-carboxyphenylboronic acid/reduced graphene oxide–gold nanocomposites[28] have been employed to fabricate AChE biosensors, which showed good performance including high sensitivity, rapid response and good stability.

It is noted that graphene sheets with a high specific surface area tend to form irreversible agglomerates through strong π–π stacking and van der Waals interactions.[29] Hence the prevention of aggregation is a key challenge in the synthesis and processing

Institute of Molecular Science, Chemical Biology and Molecular Engineering, Laboratory of Education Ministry, Shanxi University, Taiyuan 030006, P.R. China. E-mail: han_gaoyis@sxu.edu.cn; Fax: +86-351-7010699; Tel: +86-351-7010699

† Electronic supplementary information (ESI) available. See DOI: 10.1039/c2an35065c

of bulk-quantity graphene sheets. It is proved that ionic liquids (ILs) can meet this challenge well due to their wide solubility and surface charge. Functionalized graphene sheets with good dispersibility and long-term stability in various solvents have been synthesized by Yang's group.[30] In addition, IL-based electrochemical sensors and biosensors have also been extensively reported for direct electron transfer of various redox enzymes and detection of different types of compounds such as ascorbic acid, dopamine, hydrogen peroxide, and glucose.[31–34] These results suggest that the use of ILs can increase the sensitivity of response and facilitate direct electron transfer of various redox biomolecules efficiently.

As far as is known to us, AChE biosensors based on ionic liquid-functionalized graphene have not been developed. In an effort to develop a highly sensitive bio-sensing platform for OPs, we have explored the utilization of as-prepared liquid-functionalized graphene as an immobilization matrix. The immobilized AChE exhibited greater affinity to its substrate and an excellent catalytic effect on hydrolysis of ATCl. The enzyme-based biosensor was constructed for quantitative determination of carbaryl, as a model compound for OPs. The proposed biosensor showed acceptable stability and sensitivity, and had potential application in AChE-inhibitors OPs analysis and environmental monitoring.

Experimental

Materials and reagents

Acetylcholinesterase (AChE Type C3389, 500 U mg^{-1} from electric eel), acetylthiocholine chloride (ATCl) and carbaryl were purchased from Sigma-Aldrich (USA) and used as received. The ionic liquid-functionalized graphene (IL-G) was synthesized in accordance with a published procedure.[35] 0.1 M phosphate buffer solution (PBS, pH 7.4) was prepared by mixing stock standard solutions of NaH_2PO_4 and Na_2HPO_4, and adjusting the pH with 0.1 M NaOH. Chitosan (95% deacetylation) and other chemicals were of analytical grade and used without further purification, and all solutions were prepared with doubly distilled water.

Electrode preparation and modification

Prior to modification, the glassy carbon electrode (GCE) was first polished carefully to a mirror-like state with 0.3 and 0.05 μm alumina slurry and sequentially sonicated in nitric acid (v/v = 1 : 1), acetone and double-distilled water. Then the electrode was rinsed with double-distilled water and allowed to dry at room temperature.

Chitosan solution (pH = 5.0, 1.0 mg mL^{-1}) was prepared according to a previous report.[36] 1.0 mg IL-G was added to 1.0 mL of 1.0 mg mL^{-1} chitosan aqueous solution to form a homogeneous dispersion with sonication. As displayed in Scheme 1, the modified electrode was prepared by a simple casting method as follows: initially, the pretreated GCE was modified by dropping 5.0 μL of the IL-G/chitosan solution and allowed to dry in ambient air for 4 h to obtain the IL-G–CHIT/GCE modified electrode; then the obtained electrode was finally coated with 4.0 μL of AChE solution (10 mU, containing 5 mg mL^{-1} BSA to maintain the stability of AChE), which was incubated at 25 °C for 30 min; after evaporation of water, the modified electrode was washed with PBS to remove the unbound AChE, and the resulting AChE–IL-G–CHIT/GCE was stored at 4 °C. For comparison, AChE–CHIT/GCE with the same quantities of AChE was prepared by using a similar procedure.

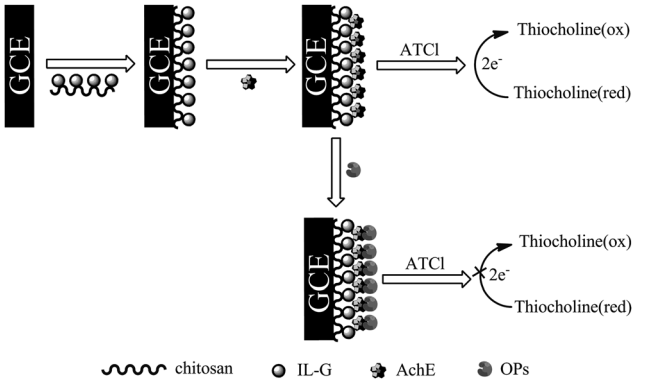

Scheme 1 Schematic representation of the biosensor fabrication and the principle for OP determination.

Measurement procedure

Inhibition by OPs: the proposed AChE–IL-G–CHIT/GCE was first immersed in 0.1 M PBS containing different concentrations of standard carbaryl solution for 8 min and then transferred to an electrochemical cell of 20.0 mL of PBS containing 1.0 mM ATCl to study the electrochemical response by cyclic voltammetry between 0.1 and 1.0 V (*versus* SCE). The inhibition of pesticide was calculated as follows: inhibition (%) = $(1 - I_{p,exp}/I_{p,control}) \times 100$, where $I_{p,control}$ is the peak current of ATCl on AChE–IL-G–CHIT/GCE and $I_{p,exp}$ is the corresponding peak current of ATCl with pesticide inhibition.

The apparent Michaelis–Menten constant (K_m) of the biosensor: the typical current–time curve was plotted for the biosensor at 750 mV after the successive addition of ATCl to 0.1 M PBS with stirring. And then the K_m value, which gives an indication of the enzyme substrate kinetics for the biosensor, was determined by analysis of the slope and intercept for the plot of the reciprocals of the steady-state current *versus* ATCl concentration.

Instrumentation

The morphologies of the obtained IL-G were observed by using a scanning electron microscope (SEM, JEOL-JSM-6701F). The UV-vis absorption spectra of IL-G aqueous solution were collected using a Hewlett-Packard HP-8453 diode spectrometer. Raman spectra were recorded on a Jobin Yvon Lab RAM HR800 microscopic confocal Raman spectrometer by employing a laser of 514 nm as the incident light. The time for each measurement was 30 s and the spectra were recorded by accumulating the measurement three times. The electrochemical experiments were performed with a CHI660 B electrochemical analyzer (Chen Hua Instruments, Shanghai, China) with a conventional three-electrode system where a GCE (3 mm in diameter) was used as the working electrode, a saturated calomel electrode (SCE) as the reference electrode and platinum wire as

the counter electrode. Electrochemical impedance spectroscopy (EIS) measurements were performed in a 0.1 M KCl solution containing 5.0 mM $Fe(CN)_6^{3-/4-}$ with a frequency range from 0.1 Hz to 100 kHz at 0.20 V, and the amplitude of the applied sine wave potential in each case was 5 mV.

Results and discussion

Characterization of IL-G

The SEM image shown in Fig. 1A illustrates that the IL-G nanosheets loaded on the electrode showed flake-like morphologies and the surface of the electrode was coarse. The graphene oxides and the IL-G were characterized by UV-vis spectroscopy before and after the reduction by $NaBH_4$. The UV-vis spectrum of graphene oxides (Fig. 1B-a) in water showed an absorption peak at 232 nm. And the absorption of water-soluble IL-G before the reduction was shifted to 252 nm (Fig. 1B-b), suggesting that the electronic conjugation within graphene sheets was restored after the functionalization by IL. After the reduction by $NaBH_4$, the absorption of IL-G red-shifted to 270 nm (Fig. 1B-c), suggesting that the electronic conjugation within graphene sheets was restored further.[29] Fig. 1C shows the Raman spectra of graphene oxides (curve a) and IL-G (curve b). It was found that the Raman spectrum of IL-G exhibited a slightly increased D/G intensity ratio relative to that of graphene oxides. This change may suggest a decrease in the average size of the sp^2 domains from IL-G and can be well explained by the creation of numerous new graphitic domains in IL-G that are smaller in size than the ones present in graphene oxides.[37]

Electrochemical impedance spectroscopy

EIS is an effective tool for studying the interface properties of surface-modified electrodes.[38] The Nyquist plot of impedance spectra includes a semicircular portion and a linear portion, and the diameter of the semicircular portion at higher frequencies is equal to the electron transfer resistance, R_{ct}, which controls the electron transfer kinetics of the redox probe at the electrode interface.[39] Fig. 2 exhibits the EIS of different electrodes in 0.1 M KCl with equimolar $Fe(CN)_6^{3-/4-}$ ions, respectively. Obviously, the R_{ct} at the IL-G–CHIT/GCE electrode (Fig. 2c) was much smaller than that at bare GCE (Fig. 2a) and CHIT/GCE (Fig. 2b), revealing that IL-G could act as a good electron-transfer interface between the electrochemical probe and the electrode.

Electrochemical behavior of AChE–IL-G–CHIT–CHIT/GCE

Cyclic voltammetry (CV) was employed to evaluate the performance of the fabricated biosensor during stepwise modification. Fig. 3A presents the CV curves of different electrodes in the absence and presence of ATCl. No peak was observed at different electrodes in 0.1 M PBS. When 1.0 mM ATCl was added, an irreversible oxidation peak at 680 mV was observed at both AChE–CHIT/GCE (curve d) and AChE–IL-G–CHIT–CHIT/GCE (curve e), which corresponded to the oxidation of thiocholine, a hydrolysis product of ATCl catalyzed by immobilized AChE.[40,41] Further observation indicated that the oxidation current of AChE to ATCl at the IL-G–CHIT–CHIT/GCE was about 4-fold higher than that at the CHIT/GCE, which was attributed to the presence of IL-G providing a conductive pathway for electron transfer.[42,43] Therefore, the IL-G–CHIT/GCE electrode was utilized for OP detection in our bio-sensing experiments.

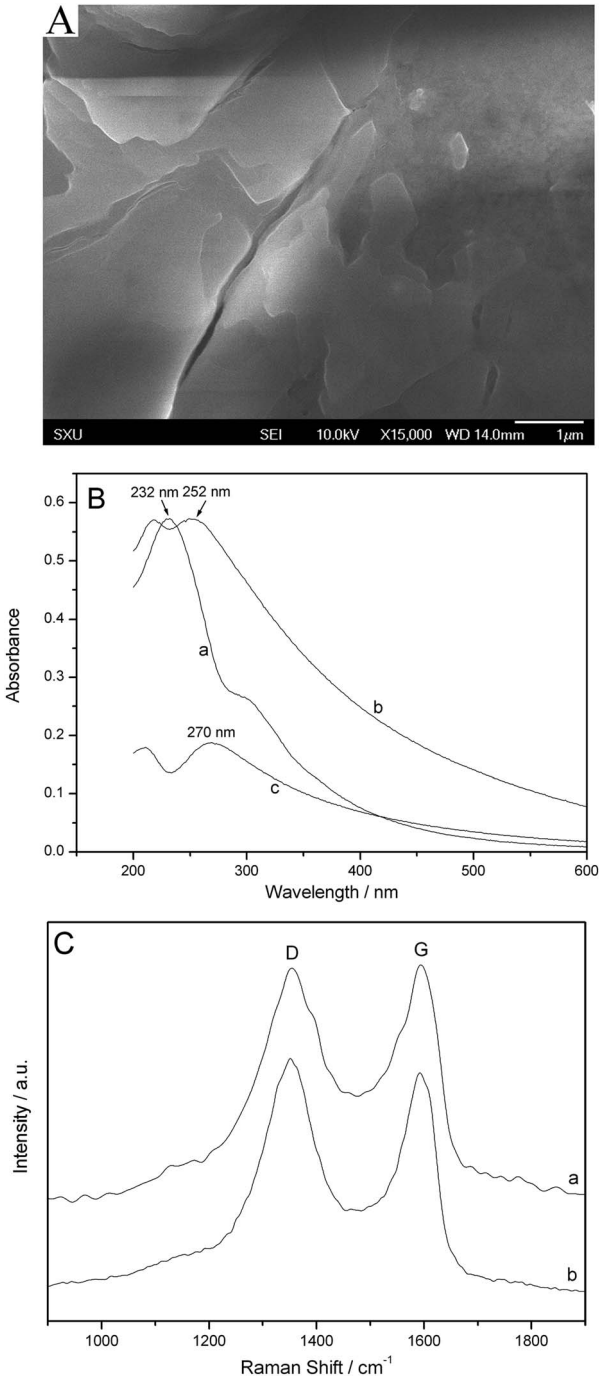

Fig. 1 (A) SEM image of IL-G. (B) The UV-vis spectra of graphene oxides (a), IL-G before (b) and after (c) the reduction with $NaBH_4$. (C) Raman spectra of graphene oxides (a) and IL-G (b).

Moreover, the effect of scan rate on the voltammetric response of immobilized AChE was also investigated. As displayed in Fig. 3B, the peak current increases while the peak potential shifts slightly with the increase of the scan rate. The peak current

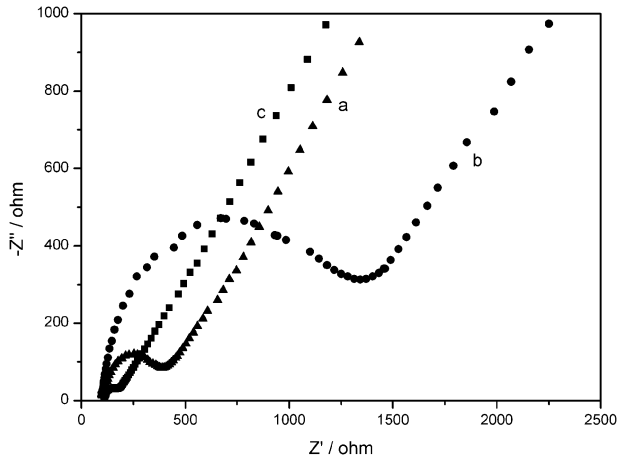

Fig. 2 EIS of (a) bare GCE, (b) CHIT/GCE and (c) IL-G–CHIT/GCE in 0.1 M KCl containing 5.0 mM $K_3[Fe(CN)_6]/K_4[Fe(CN)_6]$.

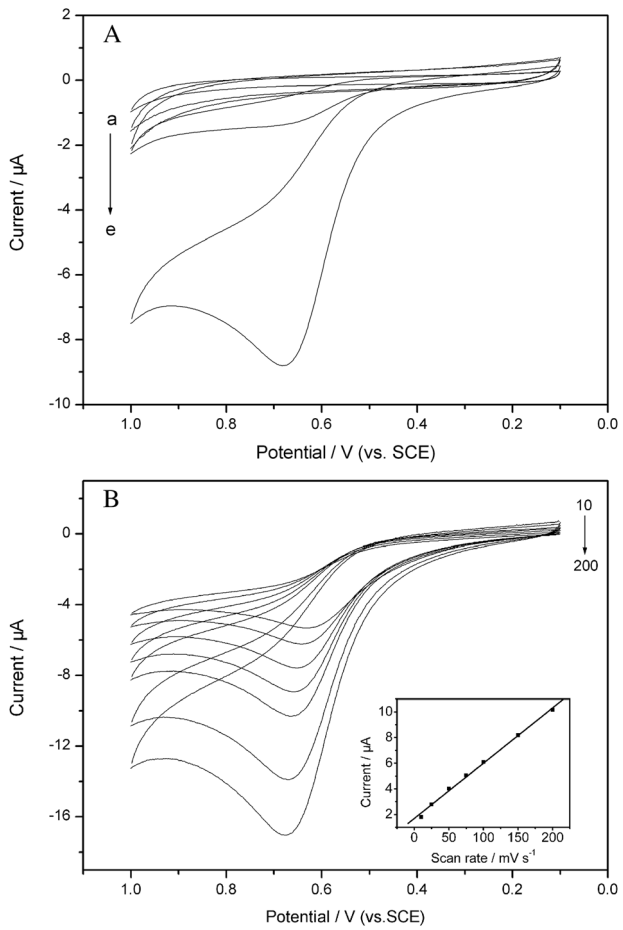

Fig. 3 (A) Cyclic voltammograms of (a) bare GCE, (b) AChE–IL-G–CHIT–CHIT/GCE in 0.1 M PBS (pH 7.4), (c) IL-G–CHIT/GCE, (d) AChE–CHIT/GCE and (e) AChE–IL-G–CHIT–CHIT/GCE in 0.1 M PBS (pH 7.4) containing 1.0 mM ATCl. Scan rate: 100 mV s^{-1}. (B) Cyclic voltammograms of AChE–IL-G–CHIT/GCE in 0.1 M PBS (pH 7.4) containing 1.0 mM ATCl at different scan rates from 10 to 200 mV s^{-1}. Inset: plots of peak current *vs.* scan rate.

exhibits a linear dependence on the scan rates ranging from 10 to 200 mV s^{-1} (inset in Fig. 3B), indicating a typical surface-controlled electrode process.[41]

Optimization parameters of the biosensor performance

The bioactivity of the immobilized AChE depended on the solution pH. Fig. 4A shows the relationship between the catalytic peak current of the response of AChE to ATCl and solution pH. Obviously, the maximum peak current was obtained at pH 7.4 in the pH range from 5.7 to 8.0. This result was close to that of a previous report for free AChE, indicating that the IL-G nanocomposite did not alter the optimal pH for the catalytic behavior of AChE and the microenvironment surrounding the immobilized enzyme was easily accessed by the substrate.[44] Thus, pH 7.4 was used for the detection solution.

The amount of AChE loaded on the electrode surface was another important parameter. Fig. 4B displays the effect of enzyme loading on the amperometric response. With increasing volume of AChE the current increased and then tended to a constant value. It can be explained that as a result of limitation of electrode area, more than 4.0 μL of enzyme adsorbing were not stable enough, indicating a saturation of enzyme loading. Therefore, a volume of 4.0 μL of AChE is chosen as the optimal volume for preparation of the biosensor.

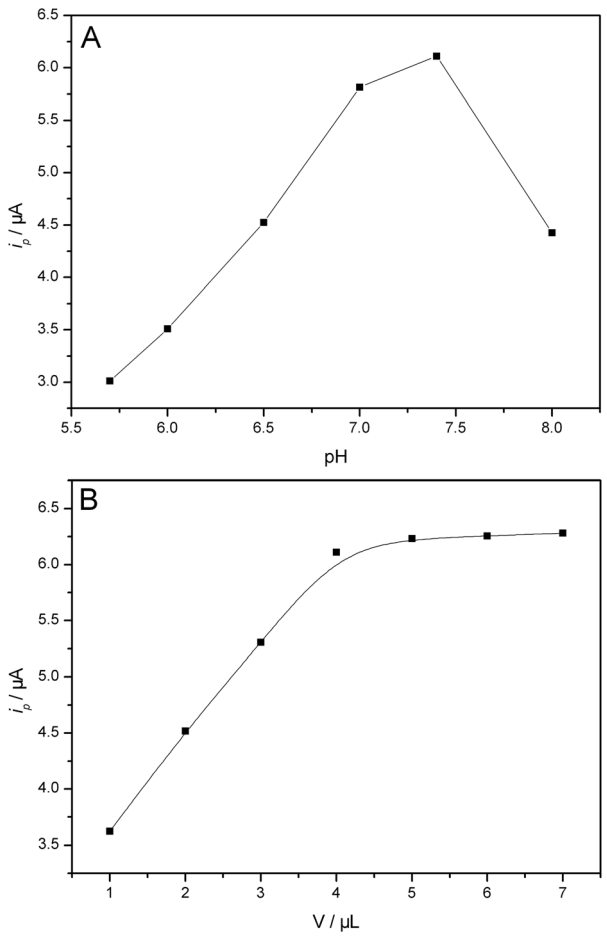

Fig. 4 Effect of the pH (A) and the volume of immobilized AChE (B) on the amperometric response.

Calibration plot of ATCl

The typical current–time response curve of the biosensor was obtained by successive additions of the substrate into a stirred cell. As displayed in Fig. 5A, with increasing concentration of ATCl, the amperometric response increased linearly in the range of 0.15–0.70 mM with a correlation coefficient of 0.999 and then tended to a plateau value, showing a typical Michaelis–Menten process (Fig. 5B). The apparent Michaelis–Menten constant (K_m) is calculated to be 0.77 mM according to the Lineweaver–Burk equation. This value was much lower than that for AChE adsorbed on a polyethyleneimine-modified electrode (1.5 mM),[45] indicating that the immobilized AChE possesses a higher enzymatic activity and affinity for ATCl due to the excellent electron transfer channels of IL-G.

Effect of incubation time on inhibition

The inhibition time is one of the most influential parameters in pesticide analysis. Therefore, the dependence of incubation time on the carbaryl inhibition was also studied. As shown in Fig. S1†, carbaryl displayed an increasing inhibition of AChE with the increase of immersion time, and when the incubation time was longer than 8 min, the curve trends to a stable value, indicating that the binding interaction with active target groups in the enzyme reaches saturation. However, the maximum value of inhibition was not 100%, which is likely attributed to the binding equilibrium between pesticides and binding sites in the enzyme.[46] Thus, an 8 min incubation time was used in subsequent experiments.

Detection of carbaryl

Based on the inhibition by OPs of the immobilized AChE activity, a simple and effective way for monitoring OPs was proposed. As shown in Fig. 6, the inhibition of carbaryl was proportional to its concentration from 0.0025 to 0.48 μg mL^{-1} and from 0.48 to 1.42 μg mL^{-1} with a detection limit of 0.8 ng mL^{-1} (S/N = 3), which was comparable with those reported electrochemical sensors.[25,26] The concentration range was wider than that of 66.4 ng mL^{-1} to 1.33 μg mL^{-1} for direct electrochemical determination of carbaryl using a multi-walled carbon nanotube/cobalt phthalocyanine-modified electrode[47] and 10 ng mL^{-1} to 1 μg mL^{-1} by flow injection–direct chemiluminescence detection.[48]

Reactivation of the biosensor

It was also observed that the as-prepared biosensor inhibited by carbaryl within a certain concentration can resume 90.5% of its original value after immersion in 0.1 M PBS (pH 7.4) for 10 min, indicating that PBS plays an important role as a reagent for AChE reactivation. Compared with nucleophilic compounds such as pralidoxime iodide as reagents of reactivation previously reported,[49] this method was simple and reliable.

Precision of measurements and stability of biosensor

The intra-assay precision of the biosensors was evaluated by assaying one enzyme electrode for five replicated determinations in 1 mM ATCl after being immersed in 0.30 μg mL^{-1} carbaryl for 8 min. Similarly, the inter-assay precision, or fabrication reproducibility, was estimated at five different electrodes. The RSDs of intra-assay and inter-assay were found to be 5.5% and 7.4%, respectively, indicating an acceptable reproducibility.

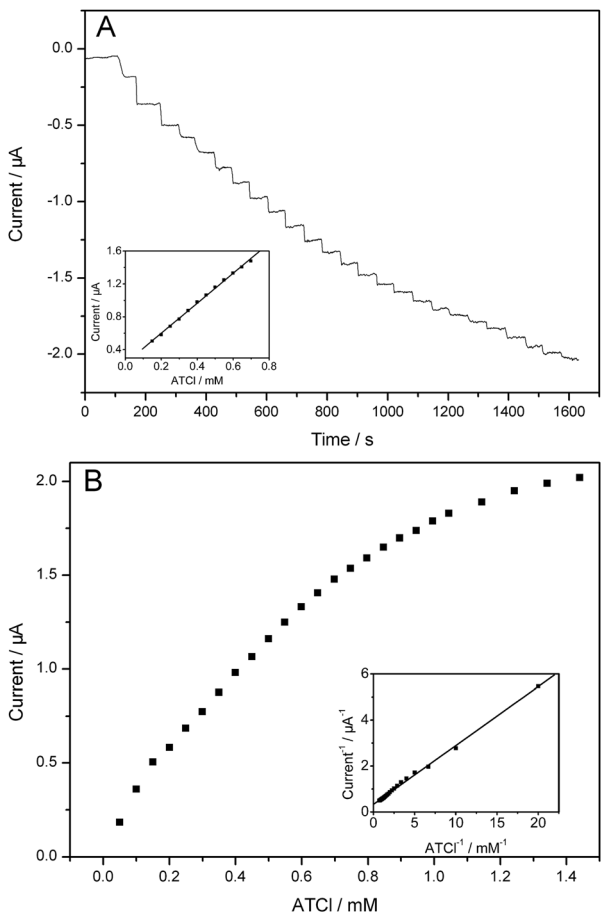

Fig. 5 (A) The *i–t* curve at AChE–IL-G–CHIT/GCE for successive addition of ATCl with stirring at the applied potential of 750 mV. Inset: the calibration plot for ATCl determination. (B) The calibration plot for the ATCl sensor. Inset: the Lineweaver–Burk plot of $1/I_{ss}$ *vs.* $1/C$.

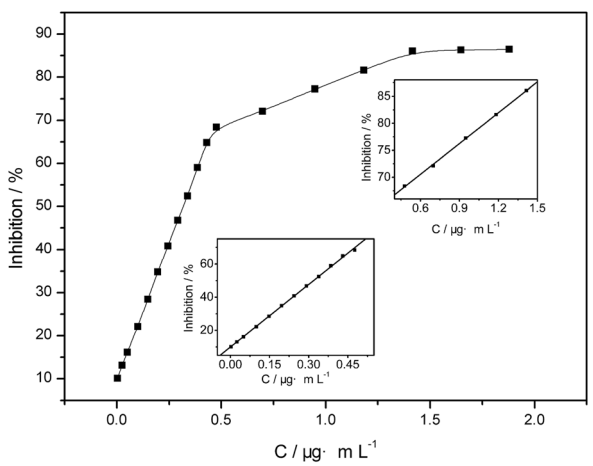

Fig. 6 Relationship between peak currents and concentrations of carbaryl. Insets: calibration plots for carbaryl determination.

Long-term storage stability was a critical issue for practical application of the proposed biosensor. When stored at 4 °C and measured at intervals of 2 days, no obvious decrease in the response of ATCl was observed in the first 7 days of storage. After a 20-day storage period, the sensor retains 85% of its initial current response, indicating an acceptable stability of the biosensor.

Conclusions

We have demonstrated a simple and efficient strategy for immobilization of AChE and developed a sensitive sensor for detection of carbaryl pesticide by integrating an IL-G nanocomposite. Due to the excellent electron-transfer channels of the nanocomposite, the immobilized AChE possesses higher enzymatic activity and affinity to ATCl. Based on the change in electrochemical response of enzymatic activity induced by OPs, an electrochemical technique with good reproducibility, acceptable stability and fast response for OPs was successfully developed. With the development of the IL-G composite in the application of carbaryl detection, we expect that the functional nanocomposite will find important and widespread applications in other OPs exposures.

Acknowledgements

The authors thank the National Natural Science Foundation of China (21073115 and 20604014), Natural Science Foundation (2007021008) of Shanxi province, the Program for New Century Excellent Talents in University (NCET-10-0926) of China and the Program for the Top Young and Middle-aged Innovative Talents of Higher Learning Institutions of Shanxi province (TYMIT and TYAL).

References

1 F. Arduini, F. Ricci, C. S. Tuta, D. Moscone, A. Amine and G. Palleschi, *Anal. Chim. Acta*, 2006, **580**, 155–162.
2 T. J. Lin, K. T. Huang and C. Y. Liu, *Biosens. Bioelectron.*, 2006, **22**, 513–518.
3 P. S. Chen and S. D. Huang, *Talanta*, 2006, **69**, 669–675.
4 S. Sotiropoulou, D. Fournier and N. A. Chaniotakis, *Biosens. Bioelectron.*, 2005, **20**, 2347–2352.
5 A. Mulchandani, P. Mulchandani, I. Kaneva and W. Chen, *Anal. Chem.*, 1998, **70**, 4140–4145.
6 G. D. Liu and Y. H. Lin, *Anal. Chem.*, 2006, **78**, 835–843.
7 J. M. Gong, L. Y. Wang and L. Z. Zhang, *Biosens. Bioelectron.*, 2009, **24**, 2285–2288.
8 D. Du, J. W. Ding, J. Cai and A. D. Zhang, *J. Electroanal. Chem.*, 2007, **605**, 53–60.
9 J. M. Gong, T. Liu, D. D. Song, X. B. Zhang and L. Z. Zhang, *Electrochem. Commun.*, 2009, **11**, 1873–1876.
10 D. Du, M. H. Wang, J. Cai and A. D. Zhang, *Sens. Actuators, B*, 2010, **146**, 337–341.
11 D. Du, W. J. Chen, J. Cai, J. Zhang, F. G. Qu and H. B. Li, *J. Electroanal. Chem.*, 2008, **623**, 81–85.
12 R. Sinha, M. Ganesana, S. Andreescu and L. Stanciu, *Anal. Chim. Acta*, 2010, **661**, 195–199.
13 A. K. Geim and K. S. Novoselov, *Nat. Mater.*, 2007, **6**, 183–191.
14 X. L. Li, G. Y. Zhang, X. D. Bai, X. M. Sun, X. R. Wang, E. Wang and H. J. Dai, *Nat. Nanotechnol.*, 2008, **3**, 538–542.
15 Y. B. Zhang, Y. W. Tan, H. L. Stormer and P. Kim, *Nature*, 2005, **438**, 201–204.
16 S. Stankovich, D. A. Dikin, G. H. B. Dommett, K. M. Kohlhaas, E. J. Zimney, E. A. Stach, R. D. Piner, S. T. Nguyen and R. S. Ruoff, *Nature*, 2006, **442**, 282–286.
17 G. Williarris, B. Seger and P. V. Kamat, *ACS Nano*, 2008, **2**, 1487–1491.
18 S. Gilje, S. Han, M. Wang, K. L. Wang and R. B. Kaner, *Nano Lett.*, 2007, **7**, 3394–3398.
19 J. S. Bunch, A. M. van der Zande, S. S. Verbridge, I. W. Frank, D. M. Tanenbaum, J. M. Parpia, H. G. Craighead and P. L. McEuen, *Science*, 2007, **315**, 490–493.
20 H. Chen, M. B. Muller, K. J. Gilmore, G. G. Wallace and D. Li, *Adv. Mater.*, 2008, **20**, 3557–3561.
21 Z. Liu, J. T. Robinson, X. M. Sun and H. J. Dai, *J. Am. Chem. Soc.*, 2008, **130**, 10876–10877.
22 N. Mohanty and V. Berry, *Nano Lett.*, 2008, **8**, 4469–4476.
23 N. G. Shang, P. Papakonstantinou, M. McMullan, M. Chu, A. Stamboulis, A. Potenza, S. S. Dhesi and H. Marchetto, *Adv. Funct. Mater.*, 2008, **18**, 3506–3514.
24 C. S. Shan, H. F. Yang, J. F. Song, D. X. Han, A. Ivaska and L. Niu, *Anal. Chem.*, 2009, **81**, 2378–2382.
25 K. Wang, Q. Liu, L. Dai, J. Yan, C. Ju, B. Qiu and X. Wu, *Anal. Chim. Acta*, 2011, **695**, 84–88.
26 K. Wang, H. N. Li, J. Wu, C. Ju, J. J. Yan, Q. Liu and B. Qiu, *Analyst*, 2011, **136**, 3349–3354.
27 Y. Wang, S. Zhang, D. Du, Y. Shao, Z. Li, J. Wang, M. H. Engelhard, J. Li and Y. Lin, *J. Mater. Chem.*, 2011, **21**, 5319–5325.
28 T. Liu, H. Su, X. Qu, P. Ju, L. Cui and S. Ai, *Sens. Actuators, B*, 2011, **160**, 1255–1261.
29 D. Li, M. B. Muller, S. Gilje, R. B. Kaner and G. G. Wallace, *Nat. Nanotechnol.*, 2008, **3**, 101–105.
30 H. Yang, C. Shan, F. Li, D. Han, Q. Zhang and L. Niu, *Chem. Commun.*, 2009, 3880–3882.
31 X. B. Lu, Q. Zhang, L. Zhang and J. H. Li, *Electrochem. Commun.*, 2006, **8**, 874–878.
32 N. Maleki, A. Safavi and F. Tajabadi, *Anal. Chem.*, 2006, **78**, 3820–3826.
33 W. Sun, D. D. Wang, R. F. Gao and K. Jiao, *Electrochem. Commun.*, 2007, **9**, 1159–1164.
34 D. Wei and A. Ivaska, *Anal. Chim. Acta*, 2008, **607**, 126–135.
35 C. S. Shan, H. F. Yang, D. X. Han, Q. X. Zhang, A. Ivaska and L. Niu, *Biosens. Bioelectron.*, 2010, **25**, 1504–1508.
36 M. G. Zhang, A. Smith and W. Gorski, *Anal. Chem.*, 2004, **76**, 5045–5050.
37 H. L. Guo, X. F. Wang, Q. Y. Qian, F. B. Wang and X. H. Xia, *ACS Nano*, 2009, **3**, 2653–2659.
38 Y. Liu, R. Yuan, Y. Q. Chai, D. P. Tang, J. Y. Dai and X. Zhong, *Sens. Actuators, B*, 2006, **115**, 109–115.
39 X. H. Kang, J. Wang, H. Wu, I. A. Aksay, J. Liu and Y. H. Lin, *Biosens. Bioelectron.*, 2009, **25**, 901–905.
40 D. Du, M. H. Wang, J. Cai, Y. H. Qin and A. D. Zhang, *Sens. Actuators, B*, 2010, **143**, 524–529.
41 D. Du, J. W. Ding, J. Cai and A. D. Zhang, *Colloids Surf., B*, 2007, **58**, 145–150.
42 K. Wang, Q. Liu, Q. M. Guan, J. Wu, H. N. Li and J. J. Yan, *Biosens. Bioelectron.*, 2011, **26**, 2252–2257.
43 D. Du, S. Z. Chen, J. Cai and A. D. Zhang, *Biosens. Bioelectron.*, 2007, **23**, 130–134.
44 M. Bernabei, S. Chiavarii, C. Cremisini and G. Palleschi, *Biosens. Bioelectron.*, 1993, **8**, 265–271.
45 P. P. Joshi, S. A. Merchant, Y. D. Wang and D. W. Schmidtke, *Anal. Chem.*, 2005, **77**, 3183–3188.
46 J. Chen, D. Du, F. Yan, H. X. Ju and H. Z. Lian, *Chem.–Eur. J.*, 2005, **11**, 1467–1472.
47 F. C. Moraes, L. H. Mascaro, S. A. S. Machado and C. M. A. Brett, *Talanta*, 2009, **79**, 1406–1411.
48 G. Z. Tsogas, D. L. Giokas, P. G. Nikolakopoulos, A. G. Vlessidis and N. P. Evmiridis, *Anal. Chim. Acta*, 2006, **573–574**, 354–359.
49 D. Du, X. Huang, J. Cai and A. D. Zhang, *Sens. Actuators, B*, 2007, **127**, 531–535.